

## Research Paper

# Effective control of tumor growth through spatial and temporal control of theranostic sodium iodide symporter (*NIS*) gene expression using a heat-inducible gene promoter in engineered mesenchymal stem cells

Mariella Tutter<sup>1</sup>, Christina Schug<sup>1</sup>, Kathrin A. Schmohl<sup>1</sup>, Sarah Urnauer<sup>1</sup>, Nathalie Schwenk<sup>1</sup>, Matteo Petrini<sup>2</sup>, Wouter J. M. Lokerse<sup>2</sup>, Christian Zach<sup>3</sup>, Sibylle Ziegler<sup>3</sup>, Peter Bartenstein<sup>3</sup>, Wolfgang A. Weber<sup>4</sup>, Ernst Wagner<sup>5</sup>, Lars H. Lindner<sup>2</sup>, Peter J. Nelson<sup>1</sup>, and Christine Spitzweg<sup>1</sup>✉

1. Department of Internal Medicine IV, University Hospital of Munich, LMU Munich, Munich, Germany
2. Department of Internal Medicine III, University Hospital of Munich, LMU Munich, Munich, Germany
3. Department of Nuclear Medicine, University Hospital of Munich, LMU Munich, Munich, Germany
4. Department of Nuclear Medicine, Klinikum rechts der Isar der Technischen Universität München, Munich, Germany
5. Department of Pharmacy, Center of Drug Research, Pharmaceutical Biotechnology, LMU Munich, Munich, Germany

✉ Corresponding author: Christine Spitzweg, MD, Department of Internal Medicine IV, University Hospital of Munich, Ludwig-Maximilians-University (LMU) Munich, Marchioninistrasse 15, 81377 Munich, Germany. Phone: +49-89-4400-0; Fax: +49-89-4400-78737; E-Mail: Christine.Spitzweg@med.uni-muenchen.de

© The author(s). This is an open access article distributed under the terms of the Creative Commons Attribution License (<https://creativecommons.org/licenses/by/4.0/>). See <http://ivyspring.com/terms> for full terms and conditions.

Received: 2019.10.25; Accepted: 2020.02.11; Published: 2020.03.15

## Abstract

**Purpose:** The tumor homing characteristics of mesenchymal stem cells (MSCs) make them attractive vehicles for the tumor-specific delivery of therapeutic agents, such as the sodium iodide symporter (NIS). NIS is a theranostic protein that allows non-invasive monitoring of the *in vivo* biodistribution of functional NIS expression by radioiodine imaging as well as the therapeutic application of <sup>131</sup>I. To gain local and temporal control of transgene expression, and thereby improve tumor selectivity, we engineered MSCs to express the *NIS* gene under control of a heat-inducible HSP70B promoter (HSP70B-NIS-MSCs).

**Experimental Design:** NIS induction in heat-treated HSP70B-NIS-MSCs was verified by <sup>125</sup>I uptake assay, RT-PCR, Western blot and immunofluorescence staining. HSP70B-NIS-MSCs were then injected i.v. into mice carrying subcutaneous hepatocellular carcinoma HuH7 xenografts, and hyperthermia (1 h at 41 °C) was locally applied to the tumor. 0 – 72 h later radioiodine uptake was assessed by <sup>123</sup>I-scintigraphy. The most effective uptake regime was then selected for <sup>131</sup>I therapy.

**Results:** The HSP70B promoter showed low basal activity *in vitro* and was significantly induced in response to heat. *In vivo*, the highest tumoral iodine accumulation was seen 12 h after application of hyperthermia. HSP70B-NIS-MSC-mediated <sup>131</sup>I therapy combined with hyperthermia resulted in a significantly reduced tumor growth with prolonged survival as compared to control groups.

**Conclusions:** The heat-inducible HSP70B promoter allows hyperthermia-induced spatial and temporal control of MSC-mediated theranostic *NIS* gene radiotherapy with efficient tumor-selective and temperature-dependent accumulation of radioiodine in heat-treated tumors.

Key words: sodium iodide symporter, regional hyperthermia, mesenchymal stem cells, gene therapy, theranostics

## Introduction

The sodium iodide symporter (NIS) is a transmembrane glycoprotein that actively co-transport two sodium and one iodide ion across the plasma membrane into the cytoplasm of thyroid follicular

cells (reviewed in [1]). The ability to accumulate and store iodide is a characteristic of thyroid tissue and a prerequisite for thyroid hormone synthesis. This feature allows the efficient treatment/curing of

thyroid cancer through the systemic administration of radioiodide [2]. NIS-expressing target cells absorb  $\beta$ -emitting radioisotopes, such as  $^{131}\text{I}$  or  $^{188}\text{Re}$ , and drive cell death via  $\beta$ -particulate radiation of the expressing cell and the neighboring tissues through bystander effects as the decaying particles have a path length of up to 2.4 mm in tissue.

Genetically targeting NIS to non-thyroidal tumor tissues has opened the prospect of transferring standard clinical protocols for radioiodine imaging and therapy to a wide range of extra-thyroidal tumor entities [3]. Following cloning of the *NIS* gene in 1996 [4], initial experiments of *ex vivo* *NIS* gene transfer [5] and local *NIS* gene delivery by intratumoral injections have been described [6]. Subsequently, a series of diverse approaches have been evaluated for the systemic *in vivo* gene transfer into non-thyroidal tumors using viruses, nanoparticles or mesenchymal stem cells (MSCs) as carriers [7-28]. To this end, adoptively applied MSCs have been demonstrated to exhibit an innate tumor tropism and have been extensively studied as potential tumor-selective gene transfer vehicles including progressing to clinical studies [29-44]. Our group initially demonstrated the efficient transfer of functional *NIS* expression with accompanying therapeutic effects using MSCs transfected with *NIS* under the control of the constitutively active CMV-promoter [34]. As a next step, to reduce potential non-tumor side effects by enhancing tumor-selective *NIS* expression, we studied the potential use of the tumor stroma-induced CCL5 (RANTES) gene promoter, which allowed a robust tumoral iodine accumulation in experimental tumors in mice leading to significantly reduced tumor growth and prolonged survival of the experimental animals after  $^{131}\text{I}$  and  $^{188}\text{Re}$  treatment [35].

To expand our strategies to include local as well as temporal control of *NIS* transgene induction and enhanced tumor selectivity of MSC-mediated *NIS* gene therapy, we engineered MSCs to express the *NIS* gene under control of a heat-inducible HSP70B promoter (HSP70B-NIS-MSCs).

Heat shock proteins (HSPs) are a heterogeneous group of molecular chaperones that includes the well-characterized 70-kDa HSP70 protein. The members of this family exhibit various cellular housekeeping and stress-related functions, such as the prevention of misaggregation, degradation, disaggregation and refolding of misfolded denatured proteins [45]. Their synthesis can be induced within minutes in response to stress, such as heat, through the trimerization of heat shock factor-1 monomers that translocate to the nucleus where they bind to heat shock elements in target gene promoters, thereby

activating a paused RNA polymerase II and allowing transcription to proceed (reviewed in [46]).

Among the different heat-responsive promoters tested for gene therapy, the human HSP70B promoter was found to have a relatively low background activity and allow a rapid high level of heat-induced transgene expression *in vitro* and *in vivo* (reviewed in [47]). It was evaluated here as a candidate gene promoter for MSC-mediated *NIS* gene therapy. In the current study, we established and evaluated the use of a stable MSC line engineered with a heat-inducible HSP70B-NIS construct for enhanced control of tumor-specific *NIS* gene therapy.

## Materials and methods

### Plasmid constructs and stable transfection of MSCs

The plasmid construct pcDNA6.2ITRNEO-HSP70B-NIS, containing the full-length *NIS* gene (cDNA kindly provided by SM Jhiang, Ohio State University, Columbus, Ohio, USA) driven by the human HSP70B promoter, two sleeping beauty transposition sites and a geneticin resistance gene, was established as described previously [43] using the MultiSite Gateway Pro Plus Kit (Thermo Fisher Scientific, Waltham, Massachusetts, USA).

Simian virus 40 large T antigen-immortalized human bone marrow-derived MSCs were used for the experiments as the immortalized MSCs have been previously shown to retain the multilineage differentiation capacity, morphology and surface antigen pattern of primary MSCs but show greater expansion potential as aging and senescence are switched off [48]. Transfection of MSCs was performed using the Neon Transfection System (Thermo Fisher Scientific) according to the manufacturer's instructions. Wild type MSCs ( $5 \times 10^5$  cells) were electroporated with a total of 3  $\mu\text{g}$  plasmid (pcDNA6.2ITRNEO-HSP70B-NIS plus pCMV(CAT) T7-SB100X, containing a sleeping beauty transposon system [provided by Z Ivics, Max Delbrück Center for Molecular Medicine, Berlin, Germany]) with a pulse voltage of 1300 Volt, a pulse width of 30 ms and a pulse number of 1. After 24 h incubation at 37 °C in a humidified CO<sub>2</sub> incubator, selection medium was added containing 1% geneticin (G-418; Invitrogen, Carlsbad, California, USA). The clone showing the highest accumulation of radioiodide in an *in vitro* iodide uptake assay (see below), reflecting functional *NIS* expression, was used for further experiments (HSP70B-NIS-MSC).

### Cell Culture

Cells were cultured in an incubator at 37 °C, with 5% (v/v) CO<sub>2</sub> atmosphere and 95% relative humidity. The human hepatocellular carcinoma (HCC) cell line

HuH7 (JCRB0403; Japanese Collection of Research Bioresources Cell Bank, Osaka, Japan) was grown in Dulbecco's Modified Eagle Medium (1 g/l glucose; Sigma Aldrich, St. Louis, Missouri, USA) supplemented with 10% (v/v) fetal bovine serum (FBS; FBS Superior, Biochrom GmbH, Berlin, Germany) and 100 U/ml penicillin and 100 µg/ml streptomycin (P/S; Sigma-Aldrich). The human MSC line (HSP70B-NIS-MSC) was cultured in Roswell Park Memorial Institute (RPMI)-1640 culture medium (Sigma-Aldrich) enriched with 10% FBS, P/S and G-418.

### **In vitro heat treatment**

For the *in vitro* hyperthermia experiments, the cell culture dishes were sealed and the cells were exposed to heat at different temperatures ranging from 39 to 42 °C in a water bath for 30 to 60 min and then maintained in an incubator at 37 °C for 4 to 48 h.

### **<sup>125</sup>I uptake assay**

NIS-mediated uptake of <sup>125</sup>I in HSP70B-NIS-MSCs was measured as described previously [49, 50]. Briefly, cells were seeded on 12-well plates and iodide uptake studies were performed at different time points (0 - 24 h) after heat treatment. Cells were incubated in Hanks' Balanced Salt solution (Gibco/Life Technologies, Carlsbad, California, USA), complemented with 10 µM NaI, 100 000 counts per minute (cpm) of Na<sup>125</sup>I/ml (PerkinElmer, Waltham, Massachusetts, USA) and 10 mM 4-(2-hydroxyethyl)-1-piperazineethanesulfonic acid (HEPES; Sigma) (pH 7.3) for 45 min. The NIS-specific inhibitor KClO<sub>4</sub> (100 mM; Merck Millipore, Burlington, Massachusetts, USA) was added to control wells to verify NIS specificity of uptake. After washing, cells were lysed in 1 N NaOH (Carl Roth GmbH + Co KG, Karlsruhe, Germany) for 15 min and trapped <sup>125</sup>I was analyzed by γ-counting (Beckman Coulter GmbH, Krefeld, Germany). Results were normalized to cell survival (see below) and expressed as cpm / A620.

### **Cell viability assay**

The commercially available MTT (3-(4,5-dimethylthiazol-2-yl)-2,5-diphenyltetrazolium bromide) assay (Sigma Aldrich) was performed following the manufacturer's instructions. The absorbance of the resulting formazan product was measured on a Sunrise microplate absorbance reader (Tecan, Männedorf, Switzerland) at a wavelength of 620 nm using the software Magellan (Tecan).

### **Quantitative real-time PCR**

Total RNA of the heat treated and control HSP70B-NIS-MSCs was isolated 0 - 48 h after thermo-stimulation using the RNeasy Mini Kit with QIAshredder (Qiagen, Venlo, Netherlands) according

to the manufacturer's recommendations. Single stranded cDNA was generated using Superscript III reverse transcriptase (Invitrogen). Quantitative real-time PCR (RT-PCR) was performed using the SYBR green PCR master mix (Qiagen) in a Mastercycler ep gradient S PCR cyler (Eppendorf, Hamburg, Germany). The following primers were used: *SLC5A5* (hNIS) (5'-TGCGGGACTTTGCAGTACATT-3') and (5'-TGCAGATAATTCCGGTGGACA-3'), *HSPA1A* (5'-GATCAACGACGGAGACAAGC-3') and (5'-GCTGCGAGTCGTTGAAGTAG-3'), *HSPA7* (5'-TTCCATGAAGTGGTTCACGA-3') and (5'-TTGACGCTGGTGTCTTTGAG-3'), and *ACTB* (β-actin) (5'-AGAAAATCTGGCACCACACC-3') and (5'-TAGCACAGCCTGGATAGCAA-3'). Levels of cDNA were normalized to the internal control β-actin. Relative expression levels were calculated using comparative ΔΔ-Ct values.

### **Membrane preparation and Western blot**

Membrane proteins from heat-treated and control cells were extracted as described previously [49] and protein concentration measured by Bradford assay (BioRad Laboratories Inc., Hercules, California, USA). Western blot analysis was conducted as reported previously [49], using a mouse monoclonal NIS-specific antibody (Merck Millipore; dilution 1:1700) overnight at 4 °C and a horse-radish peroxidase-labeled goat anti-mouse antibody (Jackson Immuno-Research Europe Ltd., Ely, UK; dilution 1:2000) for 1 h at room temperature. After 1 min incubation with enhanced chemiluminescence Western blotting detection reagent (WESTAR ETA C 2.0; Cyanagen Srl, Bologna, Italy), images were taken with an ECL ChemoCam Imager (INTAS, Göttingen, Germany). As control for protein loading, the membrane was stripped (Restore Western Blot Stripping Buffer, Thermo Fisher Scientific) and re-probed with a monoclonal anti-β-actin antibody produced in mouse (Sigma Aldrich; dilution 1:1500). The intensity of the bands was measured by densitometry using ImageJ software (NIH, Bethesda, Maryland, USA) and normalized to the β-actin loading control, expressed as the relative amount of NIS protein.

### **Immunofluorescence staining**

HSP70B-NIS-MSCs were seeded directly on FBS-coated microscope slides and grown until 60% confluent. 6 h after hyperthermia, the slides were air-dried overnight at room temperature and monolayers fixed with 80% methanol (Carl Roth) for 5 min at 4 °C, followed by 100% acetone (Carl Roth) for 2 min at -20 °C. Following blocking with 12% bovine serum albumin (Sigma-Aldrich) in phosphate-buffered saline (PBS; Sigma Aldrich) for 30 min, cells were then incubated with a primary mouse

monoclonal NIS-specific antibody (Merck Millipore; dilution 1:500) for 90 min. A secondary Cy3 AffiniPure donkey anti-rabbit IgG antibody (Jackson ImmunoResearch; dilution 1:400) and bisbenzimidazole (Hoechst; Sigma Aldrich; dilution 1:2000) to counterstain nuclei were added for 30 min. Pictures were taken using an Axiovert 135 TV fluorescence microscope in combination with an AxioCam MRm CCD camera and the AxioVision Rel. 4.8 software (Carl Zeiss Microscopy GmbH, Jena, Germany).

### **Establishment of subcutaneous HuH7 xenografts**

5 - 6 week old female CD1 nu/nu mice were bought from Charles River (Sulzfeld, Germany) and kept under specific pathogen-free conditions with *ad libitum* access to water and mouse chow. The regional governmental commission for animals (Regierung von Oberbayern, Munich, Germany) authorized all experimental protocols.

Subcutaneous (s.c.) tumors were established by s.c. injection of  $5 \times 10^6$  HuH7 cells re-suspended in 100  $\mu$ l PBS into the right flank region of the animals. Tumor volumes were determined using a caliper and calculated by the equation height  $\times$  length  $\times$  width  $\times$  0.52. When the tumor reached a volume  $> 1500$  mm<sup>3</sup> or showed signs of necrosis, mice were sacrificed.

### **In vivo regional hyperthermia**

For regional hyperthermia treatment *in vivo*, mice were anesthetized with inhalation isoflurane narcosis and placed on a water bath covered with a plastic plate that was specifically designed to allow only the tumor bearing leg to be submerged into the water through holes in the plastic cover. A rectal thermometer (Homeothermic Blanket Systems with Flexible Probe; Harvard Apparatus, Massachusetts, USA) monitored body temperature.

### **Non-invasive monitoring of in vivo NIS biodistribution**

As soon as tumors reached a volume of approximately 500 mm<sup>3</sup>,  $5 \times 10^5$  HSP70B-NIS-MSCs were injected systemically via the tail vein every second day for a total of three times. 3 days later, regional hyperthermia was applied (41 °C or, as control, 37 °C for 1 h). The mice received 18.5 MBq (0.5 mCi) of <sup>123</sup>I (GE Healthcare Buchler GmbH & Co. KG, Braunschweig, Germany) intraperitoneally (i.p.) after 0, 6, 12, 18, 24, 36, 48, and 72 h and gamma camera imaging (e.cam, Siemens, Munich, Germany) was performed using a low-energy, high-resolution collimator. Intrinsic thyroïdal iodide uptake was reduced by the addition of 5 mg/ml L-thyroxine (L-T4; Sigma Aldrich) to the drinking water ten days

before <sup>123</sup>I administration. Using the HERMES GOLD (Hermes Medical Solutions, Stockholm, Sweden) software, regions of interest were evaluated and tumoral iodide uptake was calculated and expressed as percentage of injected dose (ID) per tumor (% ID/tumor). Using the Medical Internal Radiation Dose (MIRD) concept, dosimetry was calculated with a RADAR dose factor ([www.doseinfo-radar.com](http://www.doseinfo-radar.com)).

### **Ex vivo immunohistochemical NIS protein staining**

Paraffin-embedded tumor sections and a series of control organs from the mice used for <sup>123</sup>I-scintigraphy were immunohistochemically stained as described previously [51]. Staining was performed using a primary mouse monoclonal NIS-specific antibody (Merck Millipore; dilution 1:500) for 90 min followed by a biotin-SP-conjugated goat anti-mouse IgG antibody (Jackson ImmunoResearch; dilution 1:200) for 20 min and then peroxidase-conjugated streptavidin (Jackson ImmunoResearch; dilution 1:300) for an additional 20 min. Immunohistochemically stained tumor sections were scanned using the Panoramic MIDI digital slide scanner and pictures taken with Caseviewer software (3DHISTECH Ltd., Budapest, Hungary) and control organs were imaged on an Olympus BX41 microscope equipped with an Olympus XC30 CCD camera (Olympus, Shimjukum Tokio, Japan).

### **Ex vivo mRNA expression analysis**

Frozen tumor sections of the <sup>123</sup>I-scintigraphy were shredded using 20G and 25G syringes and RNA was isolated using the RNeasy Mini Kit with QIAshredder (see above). RT-PCR was run on a Lightcycler 96 System (Roche, Basel, Switzerland) and levels of cDNA were normalized to the mean of the internal controls  $\beta$ -actin, r18S and UBC. In addition to NIS, the primers r18S (5'-CAGCCACCCGAGATTGAGCA-3') and (5'-TAGTAGCGACGGGCGGTGTG-3') and UBC (5'-ATTTGGTTCGCGGTTCTTG-3') and (5'-TGCCTTGACATTCTCGATGGT-3') were used.

### **<sup>131</sup>I-therapy study**

Therapy trials were started when tumors had an average size of 5 x 5 mm. Ten days before radioiodide injection, drinking water of mice was supplemented with L-T4 and standard mouse chow was switched to a low iodine diet (ssniff Spezialdiäten GmbH, Soest, Germany) to reduce radioiodine uptake by the thyroid gland and enhance potential tumoral iodine accumulation. Animals were randomly assigned to six treatment groups. HSP70B-NIS-MSCs were injected intravenously (i.v.) three times on every second day, followed by hyperthermia application 72 h later. 12 - 18 h after the heat treatment, 55.5 MBq (1.5 mCi) <sup>131</sup>I

(GE Healthcare) were injected i.p. This cycle was repeated 24 h after  $^{131}\text{I}$  administration, for a total of three times, with the second and third cycle consisting of only one MSC injection to reduce therapy duration (therapy group: HSP70B-NIS-MSCs + 41 °C +  $^{131}\text{I}$ ;  $n = 9$ ). To investigate the potential direct effects of hyperthermia on MSCs, we used saline instead of  $^{131}\text{I}$  (NaCl; Fresenius Kabi, Bad Homburg, Germany; HSP70B-NIS-MSCs + 41 °C + NaCl;  $n = 7$ ). In an additional control group, MSCs and radioiodide were replaced by saline (NaCl + 41 °C + NaCl;  $n = 10$ ) to investigate the potential effects of hyperthermia alone. As controls, the therapy schemes as described above were also conducted with 37 °C instead of 41 °C (HSP70B-NIS-MSCs + 37 °C +  $^{131}\text{I}$ ;  $n=10$ , HSP70B-NIS-MSCs + 37 °C + NaCl;  $n=8$ , and NaCl + 37 °C + NaCl;  $n=9$ ). The tumor volume of the mice was estimated as described above and mice were sacrificed when the tumor volume exceeded 1500 mm<sup>3</sup>.

### Ex vivo immunofluorescence assay

Immunofluorescence staining on dissected frozen tissue samples of HuH7 tumors and quantitative analysis of cellular proliferation (Ki67; Abcam, Cambridge, UK; dilution 1:200) and blood vessel density (CD31; BD Pharmingen, Heidelberg, Germany; dilution 1:100) were performed according to the protocol described previously [28]. Pictures were taken using a Leica DMI6000B microscope equipped with a Leica DFC365 FX camera and Leica MM AF software (Leica Microsystems GmbH, Wetzlar, Germany). Quantification of six visual fields per tumor section was performed using ImageJ software.

### Statistical analysis

All *in vitro* experiments were performed at least in triplicate and results are reported as mean  $\pm$  standard error of the mean (SEM), mean fold change  $\pm$  SEM or in percent. Statistical significance was tested by two-tailed Student's t-test, one-way analysis of variance (ANOVA) followed by post-hoc Tukey (honestly significant difference) test for comparison of more than two groups, two-way ANOVA followed by post-hoc Tukey test for the repeated measurements in the imaging study, or by log-rank for Kaplan-Meier survival plots.  $p$  values  $< 0.05$  were considered significant (\* $p < 0.05$ ; \*\* $p < 0.01$ ; \*\*\* $p < 0.001$ ).

## Results

### In vitro radioiodide uptake studies of HSP70B-NIS-MSCs

Radioiodide uptake assays were performed to verify functional NIS expression by HSP70B-NIS-MSCs. The HSP70B promoter showed a low basal activity (no  $^{125}\text{I}$  uptake above background levels of

unheated HSP70B-NIS-MSCs control cells) *in vitro* but showed a significantly induced expression in response to heat. Testing a temperature range from 39 to 42 °C, we observed the strongest radioiodine accumulation at 41 °C (Figure 1A). HSP70B-NIS-MSCs tolerated temperatures up to 41 °C well, but showed reduced viability yielding 71% viable cells at 42 °C (Figure 1C). In addition to temperature-dependence of NIS induction, we also characterized the time dependence of functional iodide uptake. The induction of  $^{125}\text{I}$  accumulation was found to occur rapidly after heat exposure with a maximum level reached as early as 4 h after hyperthermia application showing a 46-fold induction of iodide uptake as compared to unheated HSP70B-NIS-MSC-control cells (Figure 1B). The increase in iodide accumulation activity displayed a plateau with high uptake levels remaining for up to 15 h after heat-induced promoter activation. No significant change in cell viability was observed in response to heat in this time frame (Figure 1D). As a control, the iodide uptake was shown to be sensitive to the NIS-specific inhibitor perchlorate, demonstrating NIS dependency (Figure 1E).

### In vitro NIS mRNA and protein levels of HSP70B-NIS-MSCs

Parallel analysis of NIS mRNA levels by RT-PCR (Figure 2A) confirmed heat-induced and time-dependent NIS expression with the highest mRNA levels measured 4 h after heat treatment. Induction of mRNA expression of endogenous HSPs HSP70 (HSPA1A) (Figure 2B) and HSP70B (HSPA7) (Figure 2C) occurred in the same time frame as that seen for the NIS transgene. Western blot analysis showed a similar pattern of NIS protein expression with maximum protein levels seen 8 h after thermo-stimulation (Figure 2D). In addition, validation using immunofluorescence staining showed significant NIS-specific immunofluorescence in HSP70B-NIS-MSCs after hyperthermic treatment whereas only weak immunoreactivity was observed in non-heated, control HSP70B-NIS-MSCs, and no expression was seen in wild type MSCs (Figure 2E).

### Radioiodide biodistribution in vivo after MSC-mediated NIS gene transfer

By placing a thermo probe intratumorally, we confirmed rapid, stable and sufficient tumoral temperature ( $41.0 \pm 0.1$  °C or, as control,  $37.0 \pm 0.1$  °C respectively) delivery, while the body temperature of the mice stayed within physiological levels [data not shown]. Following these studies, subsequent analyses were conducted without the invasive tumoral probe, which could distort results as the wound caused by the probe could potentially influence MSC recruitment.

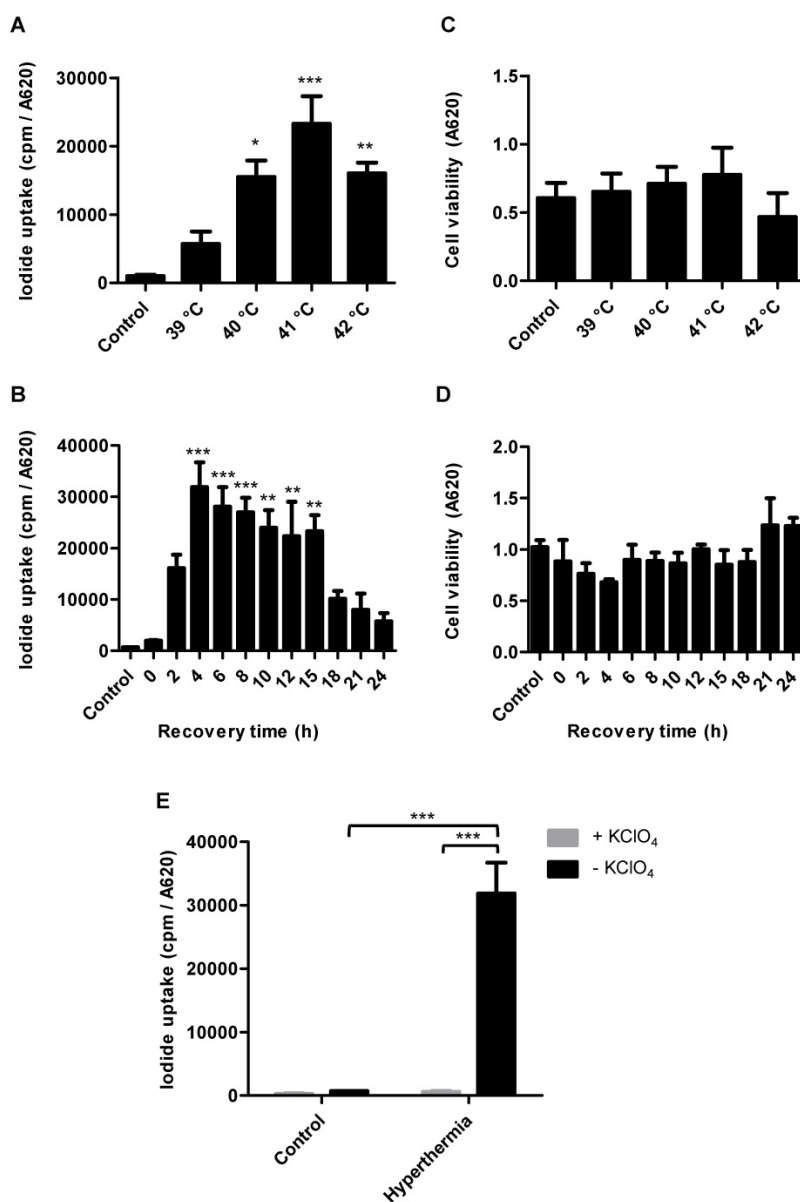


**Figure 1.** *In vitro* radioiodide uptake studies of HSP70B-NIS-MSCs. HSP70B-NIS-MSCs were heat-treated in a water bath at temperatures ranging from 39 to 42 °C for 60 min, or as control at 37 °C, and functional NIS expression was analyzed by an *in vitro* iodide uptake assay (A). <sup>125</sup>I uptake assay was performed at different time points (0–24 h) after promoter activation by heating the cells at 41 °C for 60 min (B). Cell viability after thermo-stimulation was analyzed by MTT assay (C + D). The NIS-specific inhibitor perchlorate was added to control the NIS dependency, analyzed 4 h after hyperthermia treatment and compared to unheated HSP70B-NIS-MSC control cells (E). Data are represented as mean ± SEM ( $n = 3$ ; one way ANOVA analysis; \* $p < 0.05$ ; \*\* $p < 0.01$ ; \*\*\* $p < 0.001$ ).

After three HSP70B-NIS-MSCs injections, tumor-bearing mice were heat-treated regionally for 1 h at 41 °C, to activate the heat-inducible HSP70B promoter, or as control at 37 °C. 0 to 72 h later, 18.5 MBq <sup>125</sup>I were administrated and functional NIS expression was analyzed by gamma camera imaging. The images of the <sup>125</sup>I-scintigraphy revealed the strongest tumoral iodine accumulation, mediated by functional NIS, in animals with a latency of 12 h (Figure 3C) between hyperthermia and radioiodine injection, whereas mice in the 37 °C control group (Figure 3F) exhibited the weakest signal. Quantitative analysis of serial scanning (Figure 3G) showed no difference to 37 °C control levels (maximum of tumoral iodide uptake 1 h

post <sup>125</sup>I injection [Figure 3H]: 37 °C control  $6.83 \pm 1.99\%$  ID/tumor) when radioiodine was injected directly after thermo-stimulation (Figure 3B, G-H; 0 h  $7.78 \pm 1.30\%$  ID/tumor). However, a slight increase of tumoral iodine accumulation was observed (Figure 3 G-H;  $8.58 \pm 1.86\%$  ID/tumor) when there was a period of 6 h between hyperthermia and <sup>125</sup>I injection. Significantly increased and maximal radioiodine levels were reached at the 12 h interval between promoter activation by heat treatment and radioiodide administration (Figure 3C,G-H;  $9.77 \pm 2.33\%$  ID/tumor) with a plateau up to 18 h (Figure 3G-H;  $9.41 \pm 0.86\%$  ID/tumor). All other groups, with a gap of 24 h (Figure 3D,G-H;  $7.78 \pm 0.85\%$  ID/tumor),

36 h (Figure 3G-H;  $7.99 \pm 2.22\%$  ID/tumor), 48 h (Figure 3G-H;  $6.79 \pm 0.79\%$  ID/tumor) and 72 h (Figure 3E,G-H;  $6.96 \pm 1.18\%$  ID/tumor) between HSP70B stimulation and imaging exhibited a similar iodine uptake as the control group. Physiological radioiodide accumulation in the thyroid and salivary glands (SG), stomach and, due to renal elimination of  $^{123}\text{I}$ , in the urinary bladder, was visible in all animals

(Figure 3B-F). Dosimetric calculations revealed a higher tumor-absorbed dose of  $70 \pm 28$  mGy/MBq/g tumor and an effective half-life of 3.6 h for  $^{131}\text{I}$  in heat-treated animals with the 12 h interval, as compared to the unheated control group with  $44 \pm 15$  mGy/MBq/g tumor-absorbed dose and a calculated effective half-life of 3.2 h for  $^{131}\text{I}$ .

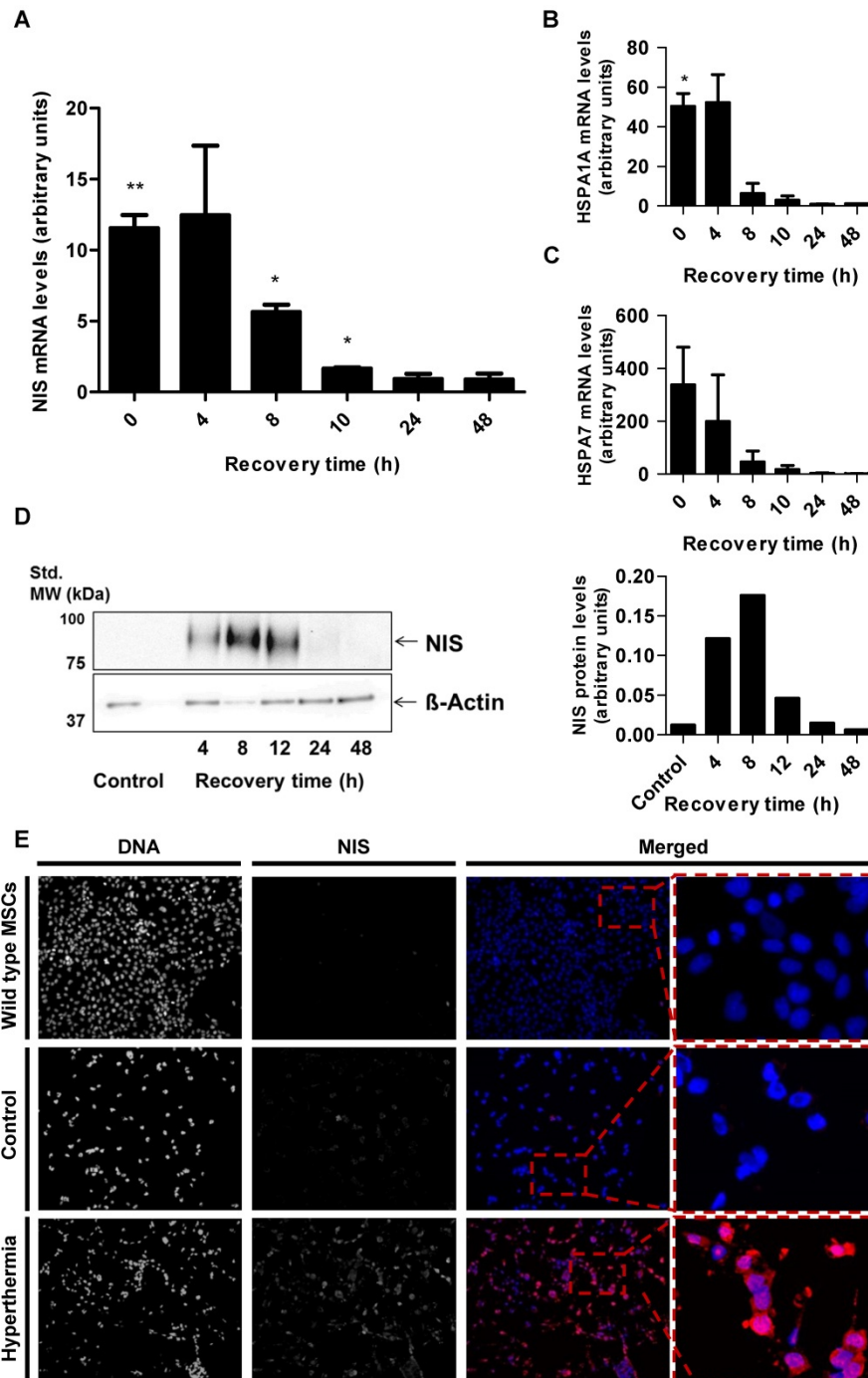


**Figure 2.** *In vitro* NIS mRNA and protein levels of HSP70B-NIS-MSCs. RT-PCR analysis of mRNA extracted from heat-treated (60 min at 41 °C) and unheated HSP70B-NIS-MSCs after 0–48 h, using primers for NIS (*SLC5A5*) (A), the endogenous HSP70 (*HSPA1A*) (B) and HSP70B (*HSPA7*) (C). Results were normalized to  $\beta$ -actin (*ACTB*), heat-treated compared to unheated MSCs for each time point and expressed as the mean  $\pm$  SEM ( $n = 3$ ; two-tailed Student's *t*-test; \* $p < 0.05$ ; \*\* $p < 0.01$ ). NIS protein levels were assessed by Western blot (D), extracted by membrane isolation at 4–48 h after thermo-stimulation or, as controls, of unheated HSP70B-NIS-MSCs. The intensity of the bands was measured by densitometry and normalized to the  $\beta$ -actin loading control. NIS-specific immunofluorescence staining (red) of heat-treated HSP70B-NIS-MSCs (bottom row), unheated HSP70B-NIS-MSCs (middle row), and unheated wild-type MSCs (top row) (E).

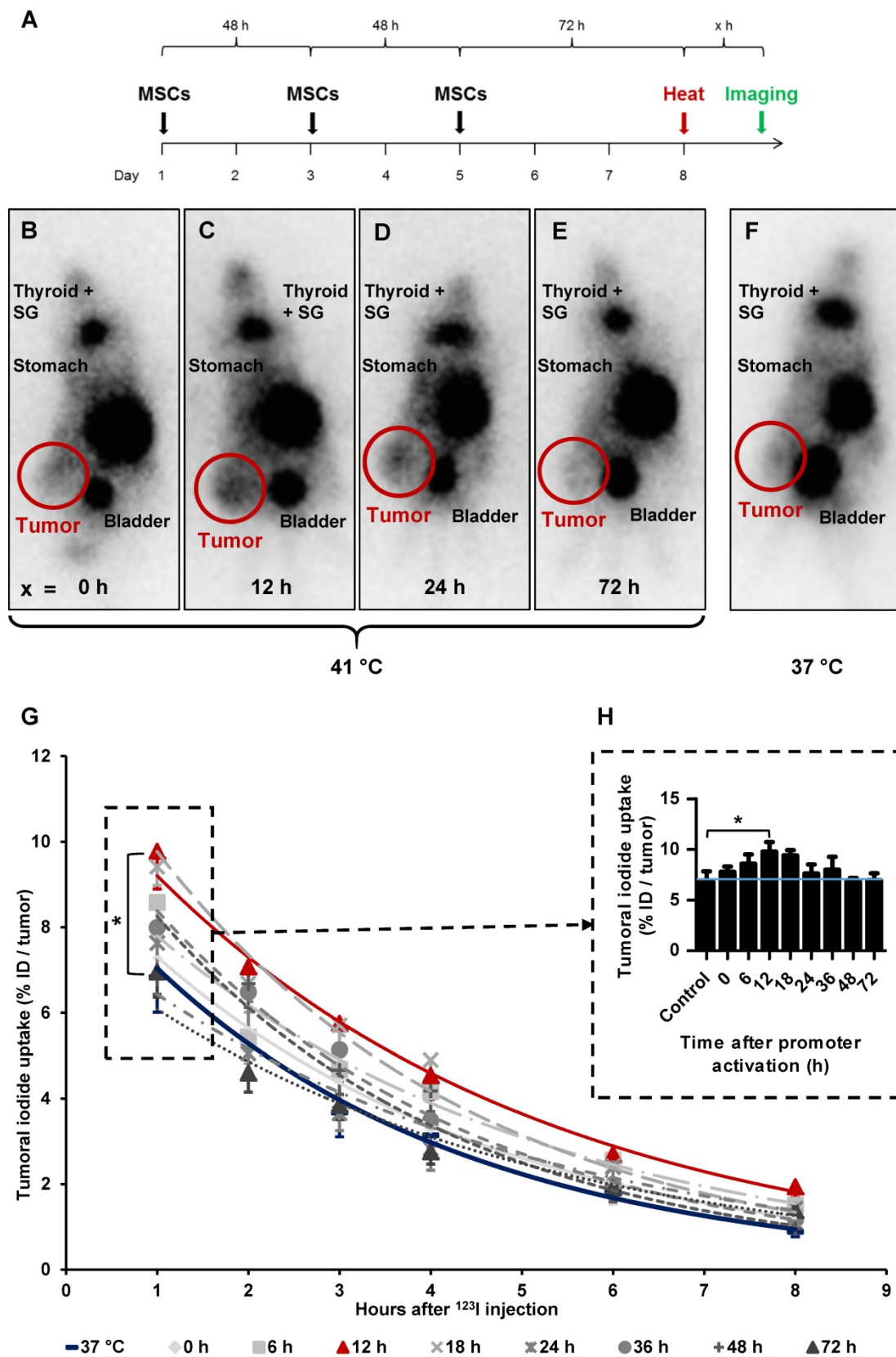


**Figure 3. Radioiodide biodistribution *in vivo* after MSC-mediated NIS gene transfer.** *In vivo*, using the hepatocellular carcinoma (HuH7) xenograft mouse model, HSP70B-NIS-MSCs were injected into the tail vein of mice, followed by hyperthermia, or as controls normothermia at 37 °C, 3 days later. 0–72 h after promoter activation by thermo-stimulation, 18.5 MBq <sup>123</sup>I were injected and serial gamma camera imaging started (A). Images of gamma camera imaging taken 2 h after radioiodide of animals with 0 h (B; n = 7), 6 h (n = 5), 12 h (C; n = 7), 18 h (n = 4), 24 h (D; n = 6), 36 h (n = 4), 48 h (n = 5) and 72 h (E; n = 4) between promoter activation by hyperthermia and radioiodine injection and control animals, treated at 37 °C (F; n = 5) (one representative image for each treatment group). Quantification of serial <sup>123</sup>I-scintigraphy (G) representing the efflux of the injected <sup>123</sup>I and comparison of the tumoral <sup>123</sup>I accumulation 1 h post injection (H) (the blue line represents the controls at 37 °C). Results are expressed as mean ± SEM; two-way ANOVA with post-hoc Tukey test \*p < 0.05.

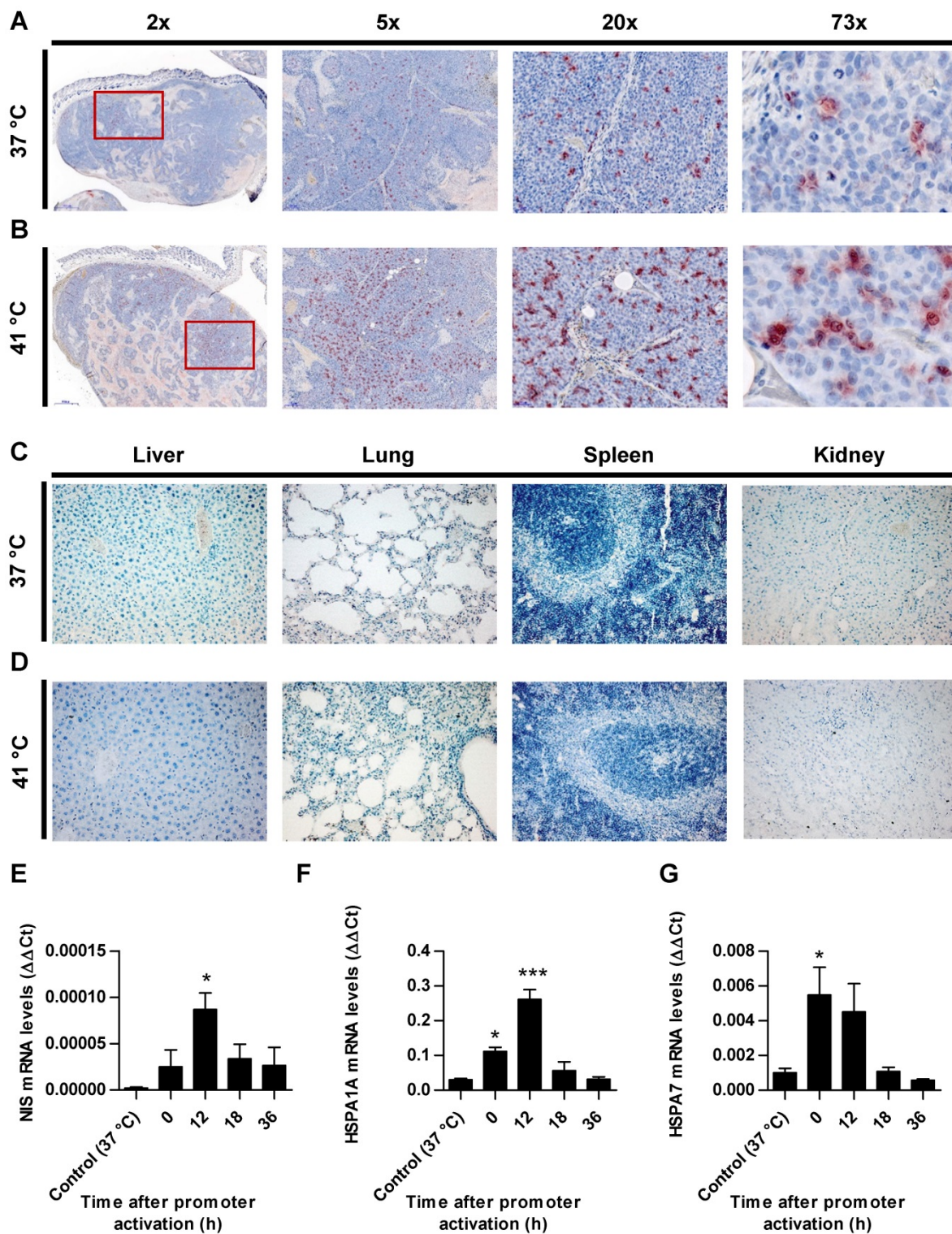


**Figure 4. Ex vivo analysis of NIS expression.** NIS-specific immunohistochemistry (red) was performed on paraffin-embedded HuH7 tumor sections. Tumors of mice of 37 °C controls (A) compared to mice which were heat-treated with a 12 h latency between promoter activation and <sup>125</sup>I administration (B). Control organs (liver, lung, spleen, and kidney) of mice receiving 37 °C (C) or 41 °C (D) treatment. One representative image is shown each at 2x – 73x magnification for tumor sections and 20x for control organs. mRNA was isolated from frozen tumors sections of heat treated mice (groups in which 0, 12, 18, and 36 h were in between promoter activation and start of <sup>125</sup>I-scintigraphy) and controls (37 °C) at the end of the serial gamma camera imaging and analyzed for NIS (E), endogenous HSPA1A (F) and HSPA7 (G) by RT-PCR (n = 4; one-way ANOVA; \*p < 0.05, \*\*\*p < 0.001).

**Ex vivo analysis of NIS expression**

Paraffin-embedded tissue sections derived from HuH7 xenografts after <sup>125</sup>I-scintigraphy were stained

immunohistochemically using a monoclonal NIS antibody. Tumor sections from control animals (37 °C; Figure 4A) showed much less perivascular human

NIS-specific immunoreaction (red) as did the group of thermo-stimulated animals (41 °C, 12 h gap; Figure 4B). Control organs (liver, lungs, spleen and kidney) of heat-treated (Figure 4D) and control animals (Figure 4C) did not show NIS-specific immunoreactivity. Frozen tumor sections were processed for mRNA isolation. RT-PCR showed an upregulation of NIS (Figure 4E), as well as the endogenous HSPs, HSP70 (Figure 4F) and HSP70B (Figure 4G) in a temperature- and time-dependent fashion as an additional confirmation of the functional NIS expression as well as the efficient heat transfer to the tumors.

### MSC-mediated NIS gene therapy *in vivo*

Following validation of functional NIS expression by non-invasive radioiodine imaging, a therapy trial with  $^{131}\text{I}$  was initiated based on the approach that showed optimal tumoral iodine accumulation as seen by the  $^{123}\text{I}$ -scintigraphy. After three MSC administrations, radioiodine was injected 12 to 18 h after hyperthermic treatment to be within the plateau phase as seen *in vitro* and by gamma camera imaging. This cycle was repeated for a total of three times, but cycle two and three consisted of only one MSC application to reduce the overall length of the treatment scheme (Figure 5A). Mice injected with saline only with (41 °C) (NaCl + 41 °C + NaCl) or without hyperthermia (37 °C) (NaCl + 37 °C + NaCl), and mice receiving saline instead of  $^{131}\text{I}$  with (41 °C) (HSP70B-NIS-MSCs + 41 °C + NaCl) and without hyperthermia (37 °C) (HSP70B-NIS-MSCs + 37 °C + NaCl), served as controls and exhibited an uninterrupted and exponential tumor growth (Figure 5B and Supplementary Figure 1). Mice treated with HSP70B-NIS-MSCs and  $^{131}\text{I}$  following hyperthermia at 41 °C (HSP70B-NIS-MSCs + 41 °C +  $^{131}\text{I}$ ) exhibited a significantly reduced tumor growth as compared to all control groups, which was associated with prolonged survival of the mice (Figure 5C). In one mouse, an impressive partial remission was observed with tumor shrinkage from 410 mm<sup>3</sup> to 28 mm<sup>3</sup> until day 78. As compared to the saline control groups, survival analysis also revealed a significantly prolonged survival of mice treated with HSP70B-NIS-MSCs of up to 78 days after therapy start in the hyperthermia group (HSP70B-NIS-MSCs + 41 °C +  $^{131}\text{I}$ ) and up to 40 days (HSP70B-NIS-MSCs + 37 °C +  $^{131}\text{I}$ ) in the normothermic group. At day 22 after the start of therapy, all animals within the NaCl + 41 °C + NaCl group had to be sacrificed based on tumor growth, whereas 100% of the HSP70B-NIS-MSCs + 41 °C +  $^{131}\text{I}$  and 70% of the HSP70B-NIS-MSCs + 37 °C +  $^{131}\text{I}$  groups were still alive. By day 26, all animals in the saline control groups had reached the endpoint criteria. The median survival after therapy start for

the therapy group HSP70B-NIS-MSCs + 41 °C +  $^{131}\text{I}$  was 31 days, for the HSP70B-NIS-MSCs + 37 °C +  $^{131}\text{I}$  25 days, for NaCl + 41 °C + NaCl treated animals 13 days, and for the NaCl + 37 °C + NaCl group 17 days. The treated mice showed no major adverse effects of radionuclide treatment and were sacrificed due to tumor load, only one mouse due to respiratory problems on day 78 after therapy start.

### Ex vivo proliferation and blood vessel density analysis

At the end of the observation period, the tumors were dissected and frozen tumor sections were stained using an antibody to identify blood vessels (CD31; red) and a Ki67-specific antibody to display general cell proliferation (green) (Figure 6A-D). Tumors treated with HSP70B-NIS-MSCs, radioiodide, and hyperthermia (HSP70B-NIS-MSCs + 41 °C +  $^{131}\text{I}$ ) (Figure 6A) showed a significantly lower proliferation index as did the saline control groups (Figure 6E), as well as a significantly lower blood vessel density compared to all three control groups (Figure 6F), thereby demonstrating an antiangiogenic effect and thus further validating successful HSP70B-NIS-MSC-mediated  $^{131}\text{I}$  therapy.

### Discussion

When used as a theranostic gene, the symporter *NIS* acts as an effective molecular reporter gene with robust therapeutic options, thus enabling the visualization and treatment of tumors through the application of appropriate radionuclides. *NIS* efficiently transports various radionuclides, allowing the application of easily available and extensively studied radionuclides such as  $^{123}\text{I}$ ,  $^{124}\text{I}$ ,  $^{18}\text{F}$ -tetrafluoroborate or  $^{99\text{m}}\text{Tc}$  for *in vivo* imaging of functional *NIS* expression, and  $^{131}\text{I}$ ,  $^{188}\text{Re}$ , or  $^{211}\text{At}$  for the delivery of therapeutic applications (summarized in [52-54]). The treatment of thyroid cancer with  $^{131}\text{I}$  has been performed in the clinic with great success since 1946 with a well-understood safety profile and is still the most preferred treatment modality, after thyroidectomy, for differentiated thyroid cancer [2]. The potential use of exogenously applied *NIS* to induce radioiodine accumulation in non-thyroidal tumors has been investigated in a variety of *in vitro* and *in vivo* tumor models, such as anaplastic thyroid cancer [55], glioma [22], acute myeloid leukemia [21], multiple myeloma [7], cancer of the prostate [6, 15, 16, 23, 56], the liver [37], the colon [27, 36], the breast [8], and the pancreas [19, 39, 57] by several groups including our own. These very promising proof-of-principle studies have led to phase I/II clinical studies with *NIS* as a reporter gene and / or therapy gene using virus-mediated *NIS* gene delivery for locally

recurrent prostate cancer (NCT00788307), multiple myeloma (NCT00450814, NCT02192775, NCT03017820), and for various other non-thyroidal cancer types

(NCT01503177, NCT01846091, NCT02364713, NCT02700230, NCT02919449, NCT02962167, NCT03120624, NCT03171493, NCT03647163) [58-61].

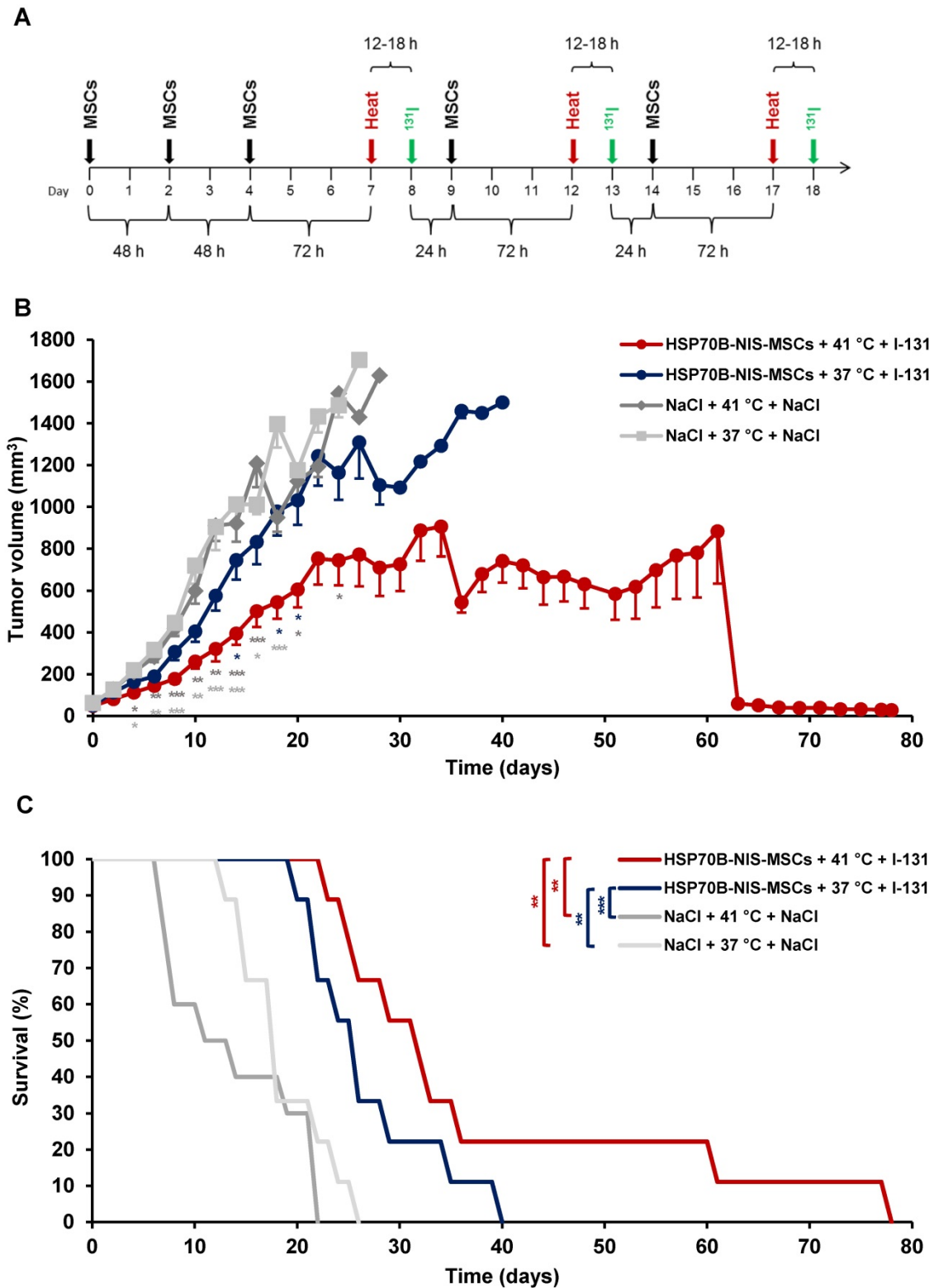


**Figure 5.** Heat-induced MSC-mediated NIS gene therapy *in vivo*. Three days after systemic injections of HSP70B-NIS-MSCs (black arrows), hyperthermia (red arrows) was administered to mice harboring HuH7 xenograft tumors. 12 to 18 h later, 55.5 MBq of therapeutic <sup>131</sup>I (green arrows) was applied. This treatment cycle was repeated for a total of three times (A). Tumor growth (B) and overall survival (C) were evaluated for the treatment with HSP70B-NIS-MSCs, hyperthermia and <sup>131</sup>I (HSP-NIS-MSCs + 41 °C + <sup>131</sup>I; n = 9), compared to control groups, receiving hyperthermia and saline (NaCl + 41 °C + NaCl; n = 10) and to normothermic groups (HSP70B-NIS-MSCs + 37 °C + <sup>131</sup>I; n = 9 and NaCl + 37 °C + NaCl; n = 10). Results are expressed as mean ± SEM (one-way ANOVA for tumor growth and log-rank test for Kaplan-Meier survival plots; \*p < 0.05; \*\*p < 0.01; \*\*\*p < 0.001).

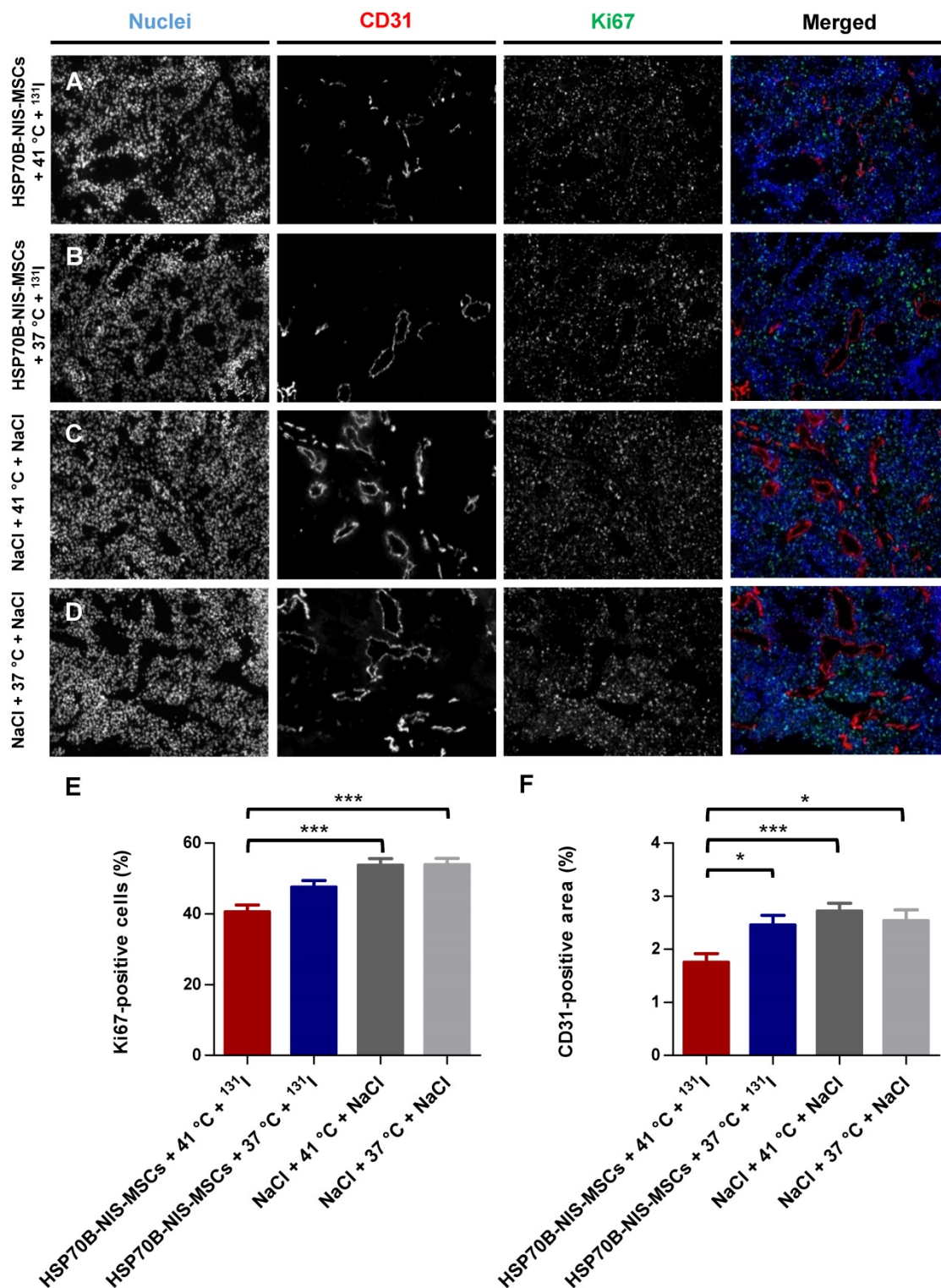


**Figure 6. Reduced ex vivo proliferation and blood vessel density as result of heat-induced MSC-mediated NIS gene therapy.** Ki67 [(E); green; proliferation index] and CD31 [(F); red; labeling blood vessels] immunofluorescence staining of frozen tumor sections was performed on tumors derived from mice receiving HSP70B-NIS-MSCs at the end of the <sup>131</sup>I therapy (A; n = 9), unheated controls (B; n = 9) and mice receiving saline with (C; n = 10) or without (D; n = 9) heat treatment instead of MSCs. Nuclei were counterstained with Hoechst (blue). One representative image is shown each at 10x magnification. Results are expressed as mean ± SEM (one-way ANOVA; \*p < 0.05; \*\*\*p < 0.001).

The ultimate goal of tumor gene therapy is the efficient delivery of a transgene by the use of systemically applied vectors. To this end, engineered versions of MSCs represent attractive candidates as

gene delivery vehicles [32]. MSCs are actively recruited to sites of tissue injuries or chronic inflammation and contribute to tissue remodeling [62]. The body sees “tumors as wounds that do not

heal” [63, 64] and for this reason it drives the mobilization of MSCs from various tissue stores and their subsequent migration to developing tumor stroma [65, 66]. MSCs exhibited selective incorporation into growing tumor stroma [67, 68] driven by high local concentrations of inflammatory chemokines and cytokines secreted by the tumor and the tumor stroma [69, 70]. This tumor tropism of MSCs has been used as a “Trojan Horse”-like therapy approach in which genetically engineered MSCs deliver a therapeutic agent, in our case the *NIS* gene, deeply into growing tumors [34-37, 39-41, 43, 71-74]. The adaption of engineered MSCs as a therapeutic approach to treat solid cancers using *NIS* has proceeded towards clinical application with the initiation of a first series of phase I/II trials using measles virus (MV)-*NIS* transfected MSCs in recurrent ovarian cancer (NCT02068794). In addition, a clinical trial using MSCs as gene delivery vehicles based on our previous work was completed using MSCs modified with CCL5-driven HSV-TK for the treatment of gastrointestinal cancer [42]. In additional clinical trials, researchers are evaluating IFN- $\beta$  expressing MSCs in ovarian cancer (NCT02530047) at MD Anderson Cancer Center, and the safety and anti-tumor capacity of TRAIL-modified MSCs in metastatic non-small cell lung cancer (NCT03298763) at University College London Hospital.

While MSCs show significant tumor tropism, a portion of the adoptively applied MSCs potentially also home to normal tissues, such as the spleen or the lung [35]. Therefore, selective control of the expression of the transgene provides a means of limiting potential damage to non-tumor tissues. Our group has demonstrated that this can be achieved by using specific gene promoters linked to signals or differentiation pathways that occur mostly or only within the tumor setting. We have previously shown that MSCs expressing *NIS* under control of the tumor stroma-specific RANTES/CCL5 promoter [35], a HIF-1 $\alpha$ -driven synthetic promoter activated by tumor hypoxia [37], or using a synthetic promoter responsive to transforming growth factor B1 (TGFB1) present in the tumor setting [43] can lead to a robust and efficient *NIS* expression within tumors. In these settings, the biodistribution of our genetically engineered MSCs was analyzed by  $^{123}\text{I}$ -scintigraphy or  $^{124}\text{I}$ - and  $^{18}\text{F}$ -TFB PET-imaging, using *NIS* as reporter gene. The subsequent systemic application of  $^{131}\text{I}$  was shown for each approach to result in a significant reduction in tumor growth and a prolonged survival of the animals, thus demonstrating both the great potential of *NIS* as a theranostic gene and the potential benefit of engineered MSCs as therapy vehicles. External beam radiation was recently found

to efficiently enhance MSC recruitment to treated tumors as well as to strongly increase tumor levels of TGFB1 [40]. Using a TGFB1-inducible SMAD-responsive promoter for MSC-mediated *NIS* gene therapy in combination with external beam radiation dramatically increased the therapeutic efficacy of *NIS* gene therapy with complete tumor remission seen in a subset of mice [41].

The present study builds on these results to evaluate a potentially more precise means of controlling theranostic transgene expression through the use of the heat-inducible HSP70B promoter that was shown here to confer local and temporal control of strong and robust induction of transgene expression. The HSP70B (*HSPA7*) gene was discovered in 1985 [75], is encoded near the highly homologous HSP70B' (*HSPA6*) on chromosome 1 [76], and, although mRNA is expressed after thermo-stimulation, it does not appear to encode a functional protein [77].

The heat-inducible HSP70B promoter was selected for use in our MSC-mediated *NIS* gene transfer approach. *In vitro* characterization of HSP70B-*NIS*-MSCs demonstrated a time- and temperature-dependent *NIS*-mediated iodine accumulation. The HSP70B promoter showed only background expression before heat was applied, but was significantly induced allowing a more than 45-fold functional *NIS* response to 60 min of heat treatment at 41 °C. *NIS* expression reached a maximum by 6 to 8 h after thermo-stimulation that was confirmed at mRNA and protein levels by RT-PCR, Western blot and *NIS*-specific immunofluorescence, respectively. These results are in line with previous studies that used the HSP70B promoter, where a similar pattern of temperature- and time-dependent promoter activity was observed *in vitro* [78-81].

We could validate these findings in an *in vivo* HCC xenograft mouse model using  $^{123}\text{I}$ -scintigraphy imaging studies that revealed a pattern of time-dependent tumoral iodine uptake, mediated by *NIS*, *in vivo* that closely matched our *in vitro* results. The strongest iodine uptake *in vivo* was found 12 h after hyperthermia treatment that was only slightly later than that seen in the cell culture studies (6 – 8 h after promoter activation). As seen with other HSP proteins that are often increased in tumor settings without thermo-stimulation due to the proteotoxic stressful conditions that cancer cells face, including nutrient deprivation, the presence of free reactive oxygen species, hypoxia, acidosis, and high levels of mutant proteins [82, 83], the HSP70B promoter (HSP70B-*NIS*-MSC) showed increased basal activity within the tumor microenvironment *in vivo* as evidenced by gamma camera images in the 37 °C

control group. This parallels the observation that HSP70 is typically found to be increased in tumors [84] and is currently evaluated as tumor-specific diagnostic and therapeutic target [85]. Importantly, the HSP70B-NIS-MSCs were not found to be activated in non-target organs (Figure 4 C + D).

Therapy using hyperthermia and  $^{131}\text{I}$  led to a strongly reduced tumor growth, prolonged survival with reduced blood vessel density and proliferation index, demonstrating the long-term antiangiogenic therapeutic efficacy of  $^{131}\text{I}$ . At normothermic conditions (37 °C), treatment with HSP70B-NIS-MSCs followed by  $^{131}\text{I}$  application resulted in slightly reduced tumor growth (22% showed a response to the therapy). HSP70B-NIS-MSCs,  $^{131}\text{I}$  and hyperthermia (41 °C) treatment resulted in a robust and significant therapeutic effect with reduced tumor growth in 67% of the animals, and a partial tumor remission in one animal. Hyperthermia and MSCs alone (HSP70B-NIS-MSCs + 41°C + NaCl) showed no difference in survival or tumor growth (Supplementary Figure 1 A +B) compared to unheated controls (HSP70B-NIS-MSCs + 37 °C + NaCl). Damage to the thyroid as well as the salivary glands is a potential and well-documented side effect of radioiodide therapy. In the present study, we used protocols similar to those used for patients that downregulate NIS expression in the thyroid gland (which is TSH regulated) by L-T4 pretreatment that helps to limit the damage to the thyroid and increases the circulating levels of radioiodide. Most of the iodide uptake in the cervical region seen on the images in Figure 3 is caused by iodide uptake in the salivary glands (that is not TSH regulated) which is anatomically close to the thyroid gland in mice and much bigger in comparison to the thyroid gland in humans [86]. Xerostomia is a recognized side effect of radioiodine treatment in some patients, but importantly, it is clinically manageable and has to be weighed against the benefit of effective tumor growth control.

One of the limitations of the present study is the somewhat heterogeneous tumoral response to hyperthermia. The therapy worked well in most of the animals, but in 33% of the animals the effect was reduced. This is believed to be due in part to the general model system applied here that used a water-based regional heat transfer method that has limitations for homogenous heat application in mouse flank tumors. This should be less of an issue in the clinic as the next generation hybrid magnetic resonance-guided high-intensity focused ultrasound now being used for tumor hyperthermia therapy allows a highly focused heating of the region with real-time temperature mapping and energy deposition [87].

As heat shows great chemo- and radiosensitizing qualities, hyperthermia has high potential as an adjuvant in multimodal treatment approaches, especially for sarcoma, melanoma, breast, or colon cancer [87]. The therapeutic effects of chemo- or radiotherapy can be enhanced by the administration of hyperthermia. Mild hyperthermia, at temperatures in the range of 39 to 44 °C, is able to disturb the *de novo* synthesis of DNA by denaturation of synthetases and polymerases resulting in arrest of the cell cycle. It can furthermore induce apoptosis or necrosis, and interfere in a number of DNA repair mechanisms [88, 89]. Recently, there is also great interest in hyperthermia in the context of oncological immunotherapy, especially in regards to the therapy of metastases. In particular, as hyperthermia can activate immune cells, initiate the release of exosomes and HSPs that present tumor antigens, enhance surface molecule expression on heated tumor cells, and thereby increase the immune sensitivity of tumors cells to the immune system. Lately, a phenomenon, called the abscopal effect, that was first discovered for local radiotherapy was now also detected for hyperthermia. It describes the findings that local tumor treatment is able to affect the growth of distant tumors and metastases and it is presumably mediated by the activation of the immune system [90].

In summary, our data demonstrate the potential of using a heat-inducible promoter (HSP70B) to drive NIS expression in MSCs, which allow an increased tumor-specific, temperature- and time-dependent NIS-mediated accumulation of radioiodide in heat-treated tumors. Application of  $^{131}\text{I}$  led to significantly reduced tumor growth and prolonged survival of animals receiving HSP70B-NIS-MSCs,  $^{131}\text{I}$  and hyperthermia. This proof-of-principle study has opened a new and exciting chapter on the way towards a future clinical application of genetically engineered MSCs in the context of *NIS* gene therapy with high translational relevance.

## Abbreviations

ANOVA: analysis of variances; CCL5: CC-chemokine ligand 5; cDNA: complementary DNA; CMV: cytomegalovirus; cpm: counts per min; DNA: deoxyribonucleic acid; FBS: fetal bovine serum; HCC: hepatocellular carcinoma; HIF1 $\alpha$ : hypoxia-inducible factor 1 $\alpha$ ; HSP: heat shock protein; HSV-TK: herpes simplex virus-thymidine kinase; ID: injected dose; i.p.: intraperitoneal; i.v.: intravenous; L-T4: L-thyroxine; MSCs: mesenchymal stem cells; mRNA: messenger ribonucleic acid; MTT: 3-(4,5-dimethylthiazol-2-yl)-2,5-diphenyltetrazolium bromide; NaCl: saline; NIS: sodium iodide symporter; PBS: phosphate-buffered saline; PET: positron-emission tomography; RANTES:

regulated on activation, normal T cell expressed and secreted; RNA: ribonucleic acid; RT-PCR: real-time polymerase chain reaction; s.c.: subcutaneous; SEM: standard error of the mean; SG: salivary glands; TGFB1: transforming growth factor beta 1.

## Supplementary Material

Supplementary figure.

<http://www.thno.org/v10p4490s1.pdf>

## Acknowledgments

We are grateful to Dr Barbara von Ungern-Sternberg, Rosel Oos, and Dr Markus Strigl (Department of Nuclear Medicine, LMU Munich, Munich, Germany), and Jakob Allmann (Department of Nuclear Medicine, Klinikum rechts der Isar der Technischen Universität München, Munich, Germany) for their support with imaging and therapy studies. The authors thank Prof Doris Mayr (Department of Pathology, LMU Munich, Munich, Germany) for preparation of paraffin-embedded slides. The authors owe special thanks to Prof Julia Mayerle, Dr Ujjwal Mahajan and Dr Ivonne Regel (Department of Internal Medicine II, LMU Munich, Munich, Germany) for always allowing the use of their equipment and giving assistance.

This work was supported by a grant from the Wilhelm Sander-Stiftung to C.S. and P.J.N. (2014.129.1), a grant from the Deutsche Forschungsgemeinschaft within the Collaborative Research Center SFB 824 to C.S. (project C8) as well as within the Priority Program SPP1629 to C.S. and P.J.N.

This work was performed as partial fulfillment of the doctoral thesis of M. Tutter at the Faculty for Chemistry and Pharmacy of the LMU Munich.

## Competing Interests

The authors have declared that no competing interest exists.

## References

- Hingorani M, Spitzweg C, Vassaux G, Newbold K, Melcher A, Pandha H, et al. The biology of the sodium iodide symporter and its potential for targeted gene delivery. *Curr Cancer Drug Targets*. 2010; 10: 242-67.
- Spitzweg C, Bible KC, Hofbauer LC, and Morris JC. Advanced radioiodine-refractory differentiated thyroid cancer: the sodium iodide symporter and other emerging therapeutic targets. *Lancet Diabetes Endocrinol*. 2014; 2: 830-42.
- Spitzweg C, Harrington KJ, Pinke LA, Vile RG, and Morris JC. Clinical review 132: The sodium iodide symporter and its potential role in cancer therapy. *J Clin Endocrinol Metab*. 2001; 86: 3327-35.
- Dai G, Levy O, and Carrasco N. Cloning and characterization of the thyroid iodide transporter. *Nature*. 1996; 379: 458-60.
- Spitzweg C, O'Connor MK, Bergert ER, Tindall DJ, Young CY, and Morris JC. Treatment of prostate cancer by radioiodine therapy after tissue-specific expression of the sodium iodide symporter. *Cancer Res*. 2000; 60: 6526-30.
- Spitzweg C, Dietz AB, O'Connor MK, Bergert ER, Tindall DJ, Young CY, et al. In vivo sodium iodide symporter gene therapy of prostate cancer. *Gene Ther*. 2001; 8: 1524-31.
- Dingli D, Peng KW, Harvey ME, Greipp PR, O'Connor MK, Cattaneo R, et al. Image-guided radiotherapy for multiple myeloma using a recombinant

- measles virus expressing the thyroidal sodium iodide symporter. *Blood*. 2004; 103: 1641-6.
- Dwyer RM, Ryan J, Havelin RJ, Morris JC, Miller BW, Liu Z, et al. Mesenchymal Stem Cell-mediated delivery of the sodium iodide symporter supports radionuclide imaging and treatment of breast cancer. *Stem Cells*. 2011; 29: 1149-57.
- Grünwald GK, Klutz K, Willhauck MJ, Schwenk N, Senekowitsch-Schmidtker R, Schwaiger M, et al. Sodium iodide symporter (NIS)-mediated radiotherapy of hepatocellular cancer using a conditionally replicating adenovirus. *Gene Ther*. 2013; 20: 625-33.
- Grünwald GK, Vetter A, Klutz K, Willhauck MJ, Schwenk N, Senekowitsch-Schmidtker R, et al. EGFR-Targeted Adenovirus Dendrimer Coating for Improved Systemic Delivery of the Theranostic NIS Gene. *Mol Ther Nucleic Acids*. 2013; 2: e131.
- Grünwald GK, Vetter A, Klutz K, Willhauck MJ, Schwenk N, Senekowitsch-Schmidtker R, et al. Systemic image-guided liver cancer radiotherapy using dendrimer-coated adenovirus encoding the sodium iodide symporter as theranostic gene. *J Nucl Med*. 2013; 54: 1450-7.
- Klutz K, Russ V, Willhauck MJ, Wunderlich N, Zach C, Gildehaus FJ, et al. Targeted radioiodine therapy of neuroblastoma tumors following systemic nonviral delivery of the sodium iodide symporter gene. *Clin Cancer Res*. 2009; 15: 6079-86.
- Klutz K, Schaffert D, Willhauck MJ, Grünwald GK, Haase R, Wunderlich N, et al. Epidermal growth factor receptor-targeted (131)I-therapy of liver cancer following systemic delivery of the sodium iodide symporter gene. *Mol Ther*. 2011; 19: 676-85.
- Klutz K, Willhauck MJ, Dohmen C, Wunderlich N, Knoop K, Zach C, et al. Image-guided tumor-selective radioiodine therapy of liver cancer after systemic nonviral delivery of the sodium iodide symporter gene. *Hum Gene Ther*. 2011; 22: 1563-74.
- Li H, Nakashima H, Decklever TD, Nace RA, and Russell SJ. HSV-NIS, an oncolytic herpes simplex virus type 1 encoding human sodium iodide symporter for preclinical prostate cancer radiotherapy. *Cancer Gene Ther*. 2013; 20: 478-85.
- Mansfield DC, Kyula JN, Rosenfelder N, Chao-Chu J, Kramer-Marek G, Khan AA, et al. Oncolytic vaccinia virus as a vector for therapeutic sodium iodide symporter gene therapy in prostate cancer. *Gene Ther*. 2016; 23: 357-68.
- Merron A, Baril P, Martin-Duque P, de la Vieja A, Tran L, Briat A, et al. Assessment of the Na/I symporter as a reporter gene to visualize oncolytic adenovirus propagation in peritoneal tumours. *Eur J Nucl Med Mol Imaging*. 2010; 37: 1377-85.
- Miller A and Russell SJ. The use of the NIS reporter gene for optimizing oncolytic virotherapy. *Expert Opin Biol Ther*. 2016; 16: 15-32.
- Penheiter AR, Wegman TR, Classic KL, Dingli D, Bender CE, Russell SJ, et al. Sodium iodide symporter (NIS)-mediated radiotherapy for pancreatic cancer. *AJR Am J Roentgenol*. 2010; 195: 341-9.
- Riesco-Eizaguirre G, De la Vieja A, Rodriguez I, Miranda S, Martin-Duque P, Vassaux G, et al. Telomerase-driven expression of the sodium iodide symporter (NIS) for in vivo radioiodide treatment of cancer: a new broad-spectrum NIS-mediated antitumor approach. *J Clin Endocrinol Metab*. 2011; 96: E1435-43.
- Shen W, Patnaik MM, Ruiz A, Russell SJ, and Peng KW. Immunovirotherapy with vesicular stomatitis virus and PD-L1 blockade enhances therapeutic outcome in murine acute myeloid leukemia. *Blood*. 2016; 127: 1449-58.
- Shi S, Zhang M, Guo R, Miao Y, and Li B. Bone Marrow-Derived Mesenchymal Stem Cell-Mediated Dual-Gene Therapy for Glioblastoma. *Hum Gene Ther*. 2019; 30: 106-117.
- Trujillo MA, Oneal MJ, McDonough S, Qin R, and Morris JC. A steep radioiodine dose response scalable to humans in sodium-iodide symporter (NIS)-mediated radiotherapy for prostate cancer. *Cancer Gene Ther*. 2012; 19: 839-44.
- Urnauer S, Morys S, Krhac Levacic A, Müller AM, Schug C, Schmohl KA, et al. Sequence-defined cMET/HGFR-targeted Polymers as Gene Delivery Vehicles for the Theranostic Sodium Iodide Symporter (NIS) Gene. *Mol Ther*. 2016; 24: 1395-404.
- Urnauer S, Klutz K, Grünwald GK, Morys S, Schwenk N, Zach C, et al. Systemic tumor-targeted sodium iodide symporter (NIS) gene therapy of hepatocellular carcinoma mediated by B6 peptide polyplexes. *J Gene Med*. 2017; 19: e2957.
- Urnauer S, Müller AM, Schug C, Schmohl KA, Tutter M, Schwenk N, et al. EGFR-targeted nonviral NIS gene transfer for bioimaging and therapy of disseminated colon cancer metastases. *Oncotarget*. 2017; 8: 92195-92208.
- Warner SG, Kim SI, Chaurasiya S, O'Leary MP, Lu J, Sivanandam V, et al. A Novel Chimeric Poxvirus Encoding hNIS Is Tumor-Tropic, Imageable, and Synergistic with Radioiodine to Sustain Colon Cancer Regression. *Mol Ther Oncolytics*. 2019; 13: 82-92.
- Urnauer S, Schmohl KA, Tutter M, Schug C, Schwenk N, Morys S, et al. Dual-targeted NIS polyplexes-a theranostic strategy toward tumors with heterogeneous receptor expression. *Gene Ther*. 2019; 26: 93-108.
- Chamberlain G, Fox J, Ashton B, and Middleton J. Concise review: mesenchymal stem cells: their phenotype, differentiation capacity, immunological features, and potential for homing. *Stem Cells*. 2007; 25: 2739-49.
- Chung T, Na J, Kim YI, Chang DY, Kim YI, Kim H, et al. Dihydropyrimidine Dehydrogenase Is a Prognostic Marker for Mesenchymal Stem Cell-Mediated

- Cytosine Deaminase Gene and 5-Fluorocytosine Prodrug Therapy for the Treatment of Recurrent Gliomas. *Theranostics*. 2016; 6: 1477-90.
31. Droujinine IA, Eckert MA, and Zhao W. To grab the stroma by the horns: from biology to cancer therapy with mesenchymal stem cells. *Oncotarget*. 2013; 4: 651-64.
  32. Hagenhoff A, Bruns CJ, Zhao Y, von Lüttichau I, Niess H, Spitzweg C, et al. Harnessing mesenchymal stem cell homing as an anticancer therapy. *Expert Opin Biol Ther*. 2016; 16: 1079-92.
  33. Karp JM and Leng Teo GS. Mesenchymal stem cell homing: the devil is in the details. *Cell Stem Cell*. 2009; 4: 206-16.
  34. Knoop K, Kolokythas M, Klutz K, Willhauck MJ, Wunderlich N, Draganovici D, et al. Image-guided, tumor stroma-targeted <sup>131</sup>I therapy of hepatocellular cancer after systemic mesenchymal stem cell-mediated NIS gene delivery. *Mol Ther*. 2011; 19: 1704-13.
  35. Knoop K, Schwenk N, Dolp P, Willhauck MJ, Zischek C, Zach C, et al. Stromal targeting of sodium iodide symporter using mesenchymal stem cells allows enhanced imaging and therapy of hepatocellular carcinoma. *Hum Gene Ther*. 2013; 24: 306-16.
  36. Knoop K, Schwenk N, Schmohl K, Müller A, Zach C, Cyran C, et al. Mesenchymal stem cell-mediated, tumor stroma-targeted radioiodine therapy of metastatic colon cancer using the sodium iodide symporter as theranostic gene. *J Nucl Med*. 2015; 56: 600-6.
  37. Müller AM, Schmohl KA, Knoop K, Schug C, Urnauer S, Hagenhoff A, et al. Hypoxia-targeted <sup>131</sup>I therapy of hepatocellular cancer after systemic mesenchymal stem cell-mediated sodium iodide symporter gene delivery. *Oncotarget*. 2016; 7: 54795-54810.
  38. Rossignoli F, Spano C, Grisendi G, Foppiani EM, Golinelli G, Mastrolia I, et al. MSC-Delivered Soluble TRAIL and Paclitaxel as Novel Combinatorial Treatment for Pancreatic Adenocarcinoma. *Theranostics*. 2019; 9: 436-448.
  39. Schug C, Gupta A, Urnauer S, Steiger K, Cheung PF, Neander C, et al. A Novel Approach for Image-Guided (<sup>131</sup>I) Therapy of Pancreatic Ductal Adenocarcinoma Using Mesenchymal Stem Cell-Mediated NIS Gene Delivery. *Mol Cancer Res*. 2019; 17: 310-320.
  40. Schug C, Sievert W, Urnauer S, Müller AM, Schmohl KA, Wechselberger A, et al. External Beam Radiation Therapy Enhances Mesenchymal Stem Cell-Mediated Sodium-Iodide Symporter Gene Delivery. *Hum Gene Ther*. 2018; 29: 1287-1300.
  41. Schug C, Kitzberger C, Sievert W, Spellerberg R, Tutter M, Schmohl KA, et al. Radiation-Induced Amplification of TGFβ1-Induced Mesenchymal Stem Cell-Mediated Sodium Iodide Symporter (NIS) Gene (<sup>131</sup>I) Therapy. *Clin Cancer Res*. 2019; 25: 5997-6008.
  42. von Einem JC, Guenther C, Volk HD, Grütz G, Hirsch D, Salat C, et al. Treatment of advanced gastrointestinal cancer with genetically modified autologous mesenchymal stem cells: Results from the phase 1/2 TREAT-ME-1 trial. *Int J Cancer*. 2019; 145: 1538-1546.
  43. Schug C, Urnauer S, Jaekel C, Schmohl KA, Tutter M, Steiger K, et al. TGFβ1-driven mesenchymal stem cell-mediated NIS gene transfer. *Endocr Relat Cancer*. 2019; 26: 89-101.
  44. Zischek C, Niess H, Ischenko J, Conrad C, Huss R, Jauch KW, et al. Targeting tumor stroma using engineered mesenchymal stem cells reduces the growth of pancreatic carcinoma. *Ann Surg*. 2009; 250: 747-53.
  45. Rosenzweig R, Nillegoda NB, Mayer MP, and Bukau B. The Hsp70 chaperone network. *Nat Rev Mol Cell Biol*. 2019; 20: 665-680.
  46. Calderwood SK, Xie Y, Wang X, Khaleque MA, Chou SD, Murshid A, et al. Signal Transduction Pathways Leading to Heat Shock Transcription. *Sign Transduct Insights*. 2010; 2: 13-24.
  47. Rome C, Couillaud F, and Moonen CT. Spatial and temporal control of expression of therapeutic genes using heat shock protein promoters. *Methods*. 2005; 35: 188-98.
  48. Gong M, Bi Y, Jiang W, Zhang Y, Chen L, Hou N, et al. Immortalized mesenchymal stem cells: an alternative to primary mesenchymal stem cells in neuronal differentiation and neuroregeneration associated studies. *J Biomed Sci*. 2011; 18: 87.
  49. Spitzweg C, Zhang S, Bergert ER, Castro MR, McIver B, Heufelder AE, et al. Prostate-specific antigen (PSA) promoter-driven androgen-inducible expression of sodium iodide symporter in prostate cancer cell lines. *Cancer Res*. 1999; 59: 2136-41.
  50. Weiss SJ, Philp NJ, and Grollman EF. Iodide transport in a continuous line of cultured cells from rat thyroid. *Endocrinology*. 1984; 114: 1090-8.
  51. Spitzweg C, Baker CH, Bergert ER, O'Connor MK, and Morris JC. Image-guided radioiodide therapy of medullary thyroid cancer after carcinoembryonic antigen promoter-targeted sodium iodide symporter gene expression. *Hum Gene Ther*. 2007; 18: 916-24.
  52. Ahn BC. Sodium iodide symporter for nuclear molecular imaging and gene therapy: from bedside to bench and back. *Theranostics*. 2012; 2: 392-402.
  53. Jiang H and DeGrado TR. [(18F)]Tetrafluoroborate [(18F)]TFB and its analogs for PET imaging of the sodium/iodide symporter. *Theranostics*. 2018; 8: 3918-3931.
  54. Ravera S, Reyna-Neyra A, Ferrandino G, Amzel LM, and Carrasco N. The Sodium/Iodide Symporter (NIS): Molecular Physiology and Preclinical and Clinical Applications. *Annu Rev Physiol*. 2017; 79: 261-289.
  55. Schmohl KA, Dolp P, Schug C, Knoop K, Klutz K, Schwenk N, et al. Reintroducing the Sodium-Iodide Symporter to Anaplastic Thyroid Carcinoma. *Thyroid*. 2017; 27: 1534-1543.
  56. Kakinuma H, Bergert ER, Spitzweg C, Chevillat JC, Lieber MM, and Morris JC. Probasin promoter (ARR(2)PB)-driven, prostate-specific expression of the human sodium iodide symporter (h-NIS) for targeted radioiodine therapy of prostate cancer. *Cancer Res*. 2003; 63: 7840-4.
  57. Schmohl KA, Gupta A, Grunwald GK, Trajkovic-Arsic M, Klutz K, Braren R, et al. Imaging and targeted therapy of pancreatic ductal adenocarcinoma using the theranostic sodium iodide symporter (NIS) gene. *Oncotarget*. 2017; 8: 33393-33404.
  58. Barton KN, Stricker H, Brown SL, Elshaikh M, Aref I, Lu M, et al. Phase I study of noninvasive imaging of adenovirus-mediated gene expression in the human prostate. *Mol Ther*. 2008; 16: 1761-9.
  59. Dispenzieri A, Tong C, LaPlant B, Lacy MQ, Laumann K, Dingli D, et al. Phase I trial of systemic administration of Edmonston strain of measles virus genetically engineered to express the sodium iodide symporter in patients with recurrent or refractory multiple myeloma. *Leukemia*. 2017; 31: 2791-2798.
  60. Galanis E, Atherton PJ, Maurer MJ, Knutson KL, Dowdy SC, Cliby WA, et al. Oncolytic measles virus expressing the sodium iodide symporter to treat drug-resistant ovarian cancer. *Cancer Res*. 2015; 75: 22-30.
  61. Russell SJ, Federspiel MJ, Peng KW, Tong C, Dingli D, Morice WG, et al. Remission of disseminated cancer after systemic oncolytic virotherapy. *Mayo Clin Proc*. 2014; 89: 926-33.
  62. Maxson S, Lopez EA, Yoo D, Danilkovitch-Miagkova A, and Leroux MA. Concise review: role of mesenchymal stem cells in wound repair. *Stem Cells Transl Med*. 2012; 1: 142-9.
  63. Foster DS, Jones RE, Ransom RC, Longaker MT, and Norton JA. The evolving relationship of wound healing and tumor stroma. *JCI Insight*. 2018; 3: e99911.
  64. Dvorak HF. Tumors: wounds that do not heal. Similarities between tumor stroma generation and wound healing. *N Engl J Med*. 1986; 315: 1650-9.
  65. Conrad C, Gupta R, Mohan H, Niess H, Bruns CJ, Kopp R, et al. Genetically engineered stem cells for therapeutic gene delivery. *Curr Gene Ther*. 2007; 7: 249-60.
  66. Niess H, Thomas MN, Schiergens TS, Kleespies A, Jauch KW, Bruns C, et al. Genetic engineering of mesenchymal stromal cells for cancer therapy: turning partners in crime into Trojan horses. *Innov Surg Sci*. 2016; 1: 19-32.
  67. Hall B, Andreeff M, and Marini F. The participation of mesenchymal stem cells in tumor stroma formation and their application as targeted-gene delivery vehicles. *Handb Exp Pharmacol*. 2007; 263-83.
  68. Kidd S, Spaeth E, Dembinski JL, Dietrich M, Watson K, Klopp A, et al. Direct evidence of mesenchymal stem cell tropism for tumor and wounding microenvironments using in vivo bioluminescent imaging. *Stem Cells*. 2009; 27: 2614-23.
  69. Spaeth E, Klopp A, Dembinski J, Andreeff M, and Marini F. Inflammation and tumor microenvironments: defining the migratory itinerary of mesenchymal stem cells. *Gene Ther*. 2008; 15: 730-8.
  70. Ponte AL, Marais E, Gallay N, Langonne A, Delorme B, Herault O, et al. The in vitro migration capacity of human bone marrow mesenchymal stem cells: comparison of chemokine and growth factor chemotactic activities. *Stem Cells*. 2007; 25: 1737-45.
  71. Chulpanova DS, Kitaeva KV, Tazetdinova LG, James V, Rizvanov AA, and Solovyeva VV. Application of Mesenchymal Stem Cells for Therapeutic Agent Delivery in Anti-tumor Treatment. *Front Pharmacol*. 2018; 9: 259.
  72. Dwyer RM, Khan S, Barry FP, O'Brien T, and Kerin MJ. Advances in mesenchymal stem cell-mediated gene therapy for cancer. *Stem Cell Res Ther*. 2010; 1: 25.
  73. Krueger TEG, Thorek DLJ, Denmeade SR, Isaacs JT, and Brennen WN. Concise Review: Mesenchymal Stem Cell-Based Drug Delivery: The Good, the Bad, the Ugly, and the Promise. *Stem Cells Transl Med*. 2018; 7: 651-663.
  74. Schmohl KA, Mueller AM, Dohmann M, Spellerberg R, Urnauer S, Schwenk N, et al. Integrin alphavbeta3-Mediated Effects of Thyroid Hormones on Mesenchymal Stem Cells in Tumor Angiogenesis. *Thyroid*. 2019; 29: 1843-1857.
  75. Voellmy R, Ahmed A, Schiller P, Bromley P, and Rungger D. Isolation and functional analysis of a human 70,000-dalton heat shock protein gene segment. *Proc Natl Acad Sci U S A*. 1985; 82: 4949-53.
  76. Leung TK, Hall C, Rajendran M, Spurr NK, and Lim L. The human heat-shock genes HSPA6 and HSPA7 are both expressed and localize to chromosome 1. *Genomics*. 1992; 12: 74-9.
  77. Parsian AJ, Sheren JE, Tao TY, Goswami PC, Malyapa R, Van Rheeden R, et al. The human Hsp70B gene at the HSPA7 locus of chromosome 1 is transcribed but non-functional. *Biochim Biophys Acta*. 2000; 1494: 201-5.
  78. Brade AM, Ngo D, Szmítko P, Li PX, Liu FF, and Klamut HJ. Heat-directed gene targeting of adenoviral vectors to tumor cells. *Cancer Gene Ther*. 2000; 7: 1566-74.
  79. Braiden U, Ohtsuru A, Kawashita Y, Miki F, Sawada T, Ito M, et al. Eradication of breast cancer xenografts by hyperthermic suicide gene therapy under the control of the heat shock protein promoter. *Hum Gene Ther*. 2000; 11: 2453-63.
  80. Liu Y, Kon T, Li C, and Zhong P. High intensity focused ultrasound-induced gene activation in solid tumors. *J Acoust Soc Am*. 2006; 120: 492-501.
  81. Smith RC, Machluf M, Bromley P, Atala A, and Walsh K. Spatial and temporal control of transgene expression through ultrasound-mediated induction of the heat shock protein 70B promoter in vivo. *Hum Gene Ther*. 2002; 13: 697-706.
  82. Balogi Z, Multhoff G, Jensen TK, Lloyd-Evans E, Yamashita T, Jäättelä M, et al. Hsp70 interactions with membrane lipids regulate cellular functions in health and disease. *Prog Lipid Res*. 2019; 74: 18-30.

83. Siddiqui F, Avery PR, Li CY, Zhang X, LaRue SM, Dewhirst MW, et al. Induction of the human heat shock promoter HSP70B by nutritional stress: implications for cancer gene therapy. *Cancer Invest.* 2008; 26: 553-61.
84. Multhoff G, Botzler C, Wiesnet M, Muller E, Meier T, Wilmanns W, et al. A stress-inducible 72-kDa heat-shock protein (HSP72) is expressed on the surface of human tumor cells, but not on normal cells. *Int J Cancer.* 1995; 61: 272-9.
85. Stangl S, Tei L, De Rose F, Reder S, Martinelli J, Sievert W, et al. Preclinical Evaluation of the Hsp70 Peptide Tracer TPP-PEG24-DFO[<sup>89</sup>Zr] for Tumor-Specific PET/CT Imaging. *Cancer Res.* 2018; 78: 6268-6281.
86. Schmohl KA, Müller AM, Schwenk N, Knoop K, Rijntjes E, Köhrle J, et al. Establishment of an Effective Radioiodide Thyroid Ablation Protocol in Mice. *Eur Thyroid J.* 2015; 4: 74-80.
87. Datta NR, Ordonez SG, Gaipal US, Paulides MM, Crezee H, Gellermann J, et al. Local hyperthermia combined with radiotherapy and/or chemotherapy: recent advances and promises for the future. *Cancer Treat Rev.* 2015; 41: 742-53.
88. Issels R, Kampmann E, Kanaar R, and Lindner LH. Hallmarks of hyperthermia in driving the future of clinical hyperthermia as targeted therapy: translation into clinical application. *Int J Hyperthermia.* 2016; 32: 89-95.
89. Hildebrandt B, Wust P, Ahlers O, Dieing A, Sreenivasa G, Kerner T, et al. The cellular and molecular basis of hyperthermia. *Crit Rev Oncol Hematol.* 2002; 43: 33-56.
90. Lee S, Son B, Park G, Kim H, Kang H, Jeon J, et al. Immunogenic Effect of Hyperthermia on Enhancing Radiotherapeutic Efficacy. *Int J Mol Sci.* 2018; 19: e2795.